Dust in a sample of about 100 LBGs and ALPINE galaxies at 4.5 < z < 6.2 observed with ALMA

Astronomy & Astrophysics manuscript no. output
October 27, 2021
©ESO 2021

The ALMA-ALPINE [CII] survey: the star formation history and the dust emission of star-forming galaxies at 4.5 < z < 6.2

D. Burgarella[1], J. Bogdanoska[1], A. Nanni[2], S. Bardelli[3], M. Béthermin[1], M. Boquien[4], V. Buat[1], A. L. Faisst[5], M. Dessauges-Zavadsky[6], Y. Fudamoto[7,8], S. Fujimoto[9,10], M. Giavalisco[11], M. Ginolfi[12], C. Gruppioni[13], N. P. Hathi[14], E. Ibar[15], G. C. Jones[16,17], A. M. Koekemoer[14], K. Kohno[18,19], B. C. Lemaux[20], D. Narayanan[21], P. Oesch[6], M. Ouchi[22,23], D. A. Riechers[24], F. Pozzi[13], M. Romano[25,26], D. Schaerer[6,27], M. Talia[3,13], P. Theulé[1], D. Vergani[3], G. Zamorani[3], and the ALPINE team

Some information about this Work

- We wished to perform SED fitting on a large sample of high-redshift star-forming galaxies (i.e. on the Main Sequence of star-forming galaxies).
- Because only a few data (meaning *detections*) is available in the far-infrared, we attempt to densify the IR SED.
- For this, we combined individual detections to build an IR composite SED. To do this, we need to make sure that the sample is homogeneous.
- Once the IR composite sample is built, we assume it to be valid for the entire sample (detections and upper limits).
- We use CIGALE to derive physical parameters, to build diagnostic diagrams and to study the stellar populations and the dust properties.

The Life Cycle of Dust Grains

outside & *inside*

OUTFLOW

Galaxies

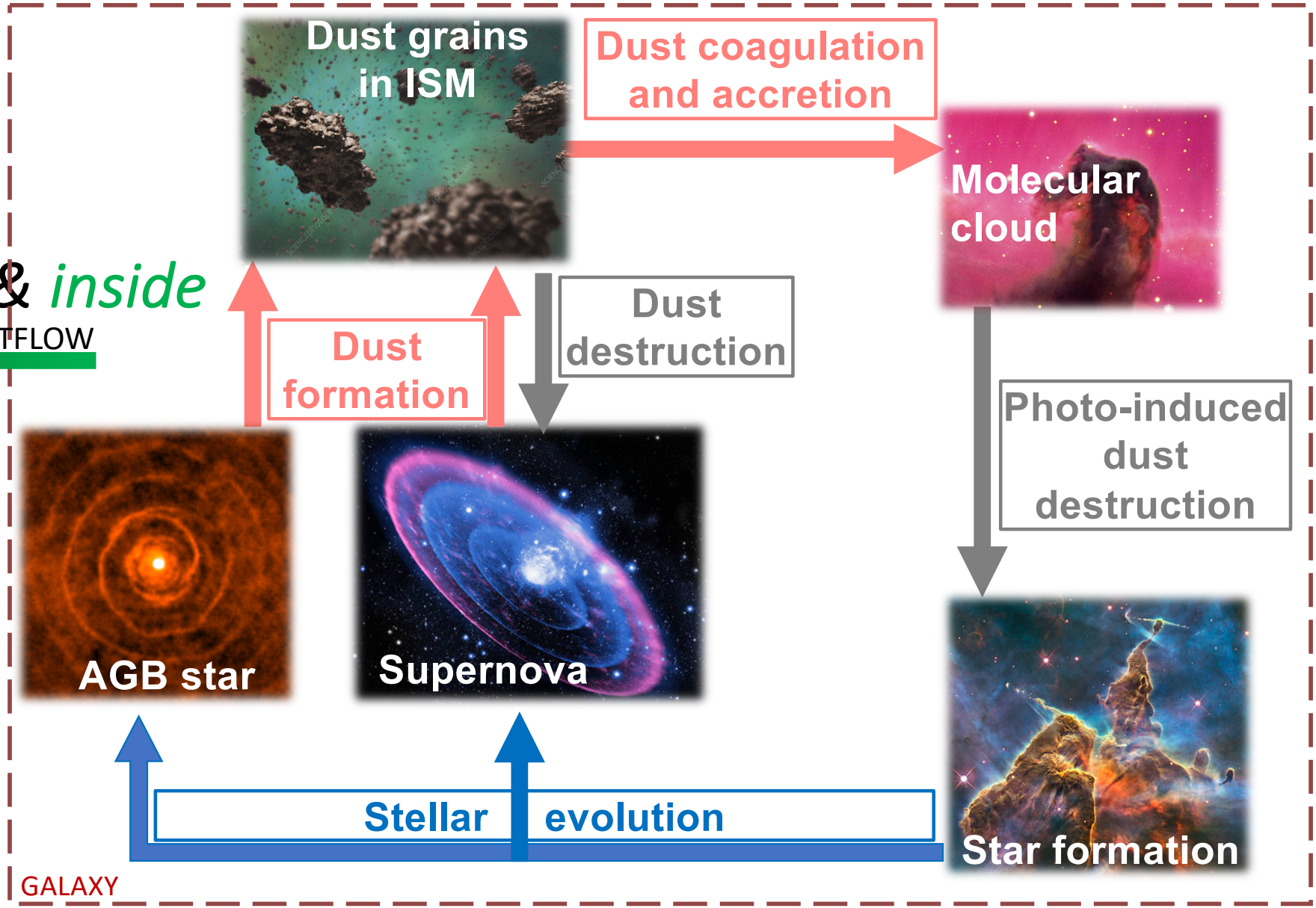

The sample of objects

Source	Number of objects	Selection	redshift	Notes
Le Fèvre et al. (2020); Faisst et al. (2020); Bethermin et al. (2020)	118	SFG	z ~ 4.5 z ~ 5.5	* 20 ALMA-7 detections with S/N > 3 * 78 ALMA-7 upper limits * 18 ALMA-7 not selected (not enough data) * $S/N_{UV-optical-NIR} > 2.5$. * SFG with > 5 data points in UV-optical only * [CII]158μm measurements for 64% of the sample
Capak et al. (2015) & Faisst et al. (2017)	4 (HZ4, HZ6, HZ9, HZ10	UV	z ~ 5.6	* [CII]158μm for all Hi-z LBGs * ALMA-7 detections: HZ4, HZ6 (3) HZ9 & HZ10 (5) * ALMA-7 upper limits for the others * HZ5 detected in Chandra and not included in the sample * Additional data from Pavesi et al. (2016)
Scoville et al. (2016)	1 (566428)	UV	z = 5.89	* ALMA-6 detection * [CII]158μm measurement
Willott et al. (2015)	2 (CLM1 & WMH5)	UV	z ~ 6.1	* ALMA-6 detections * [CII]158μm measurement

Table 1: Origins of the data used in this paper. The total sample contains 27 objects with ALMA detections, including 7 LBGs from Burgarella et al. (2020), out of a total sample of 124 objects. The final sample used in this paper contains 105 objects (27 with ALMA detections, 78 with ALMA upper limits and 18 without enough data in the UV-optical-near-IR range to perform a safe SED fitting).

Using the universe and the redshift as a spectrograph

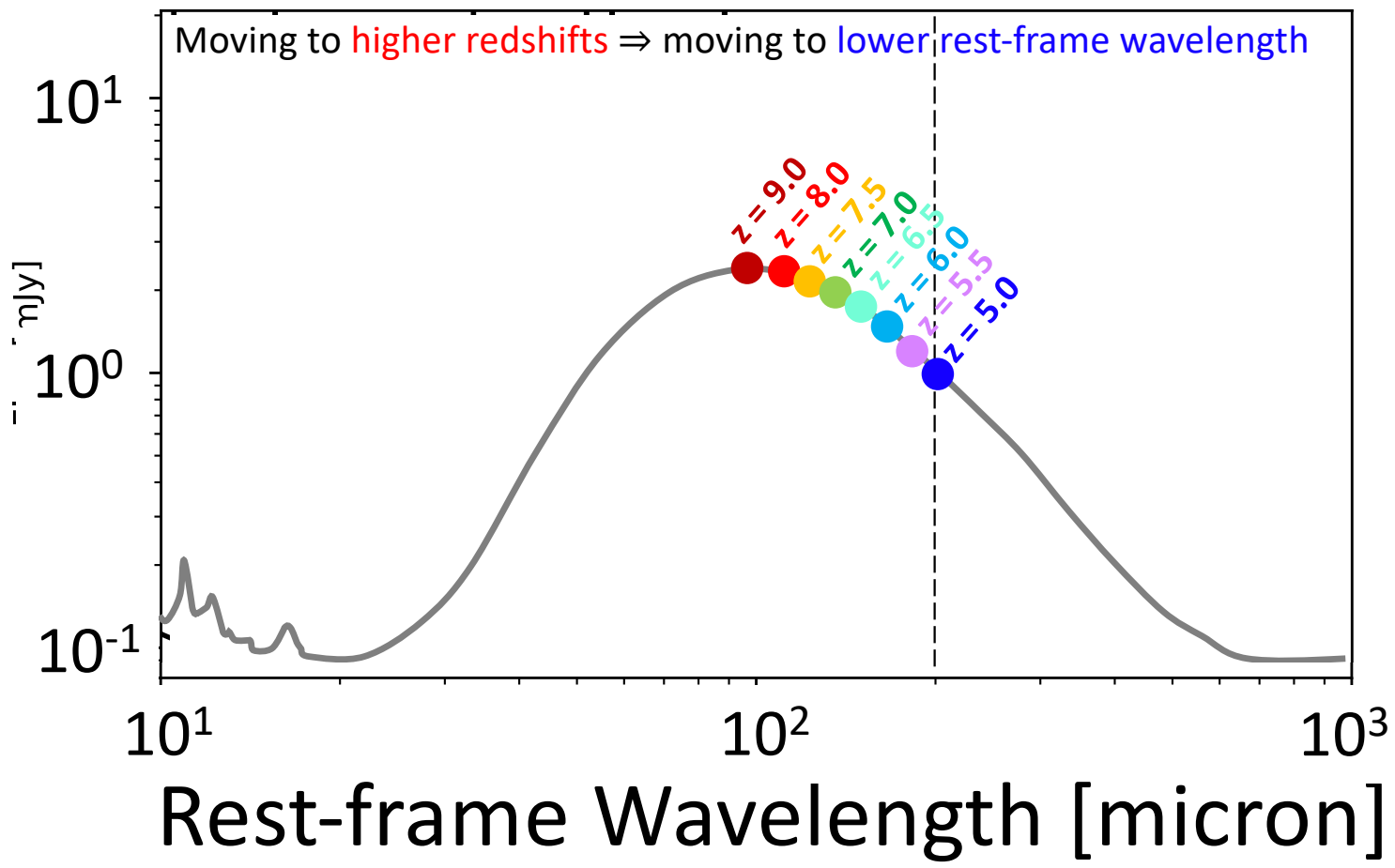

Using the universe and the redshift as a spectrograph

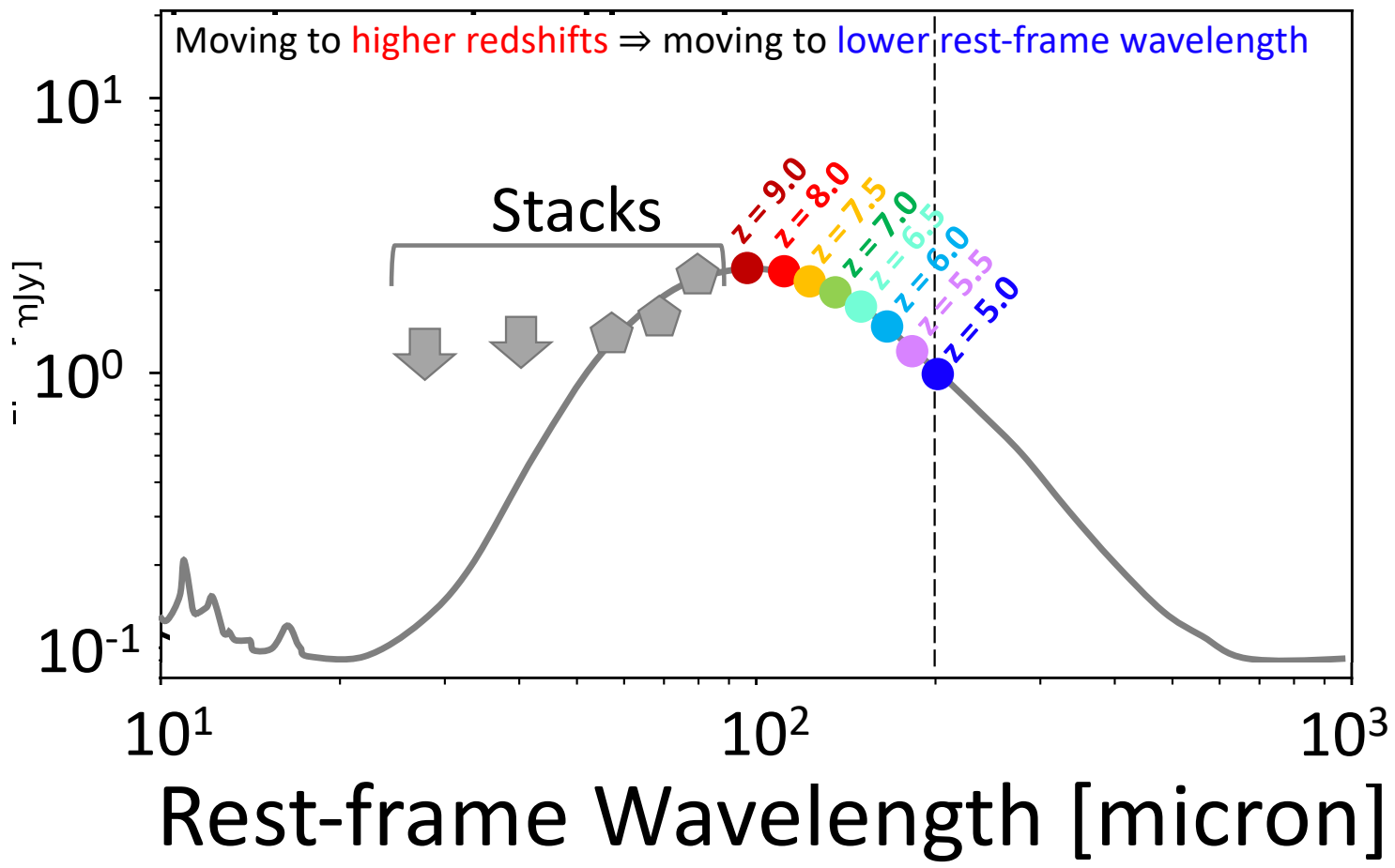

Flowchart of the project

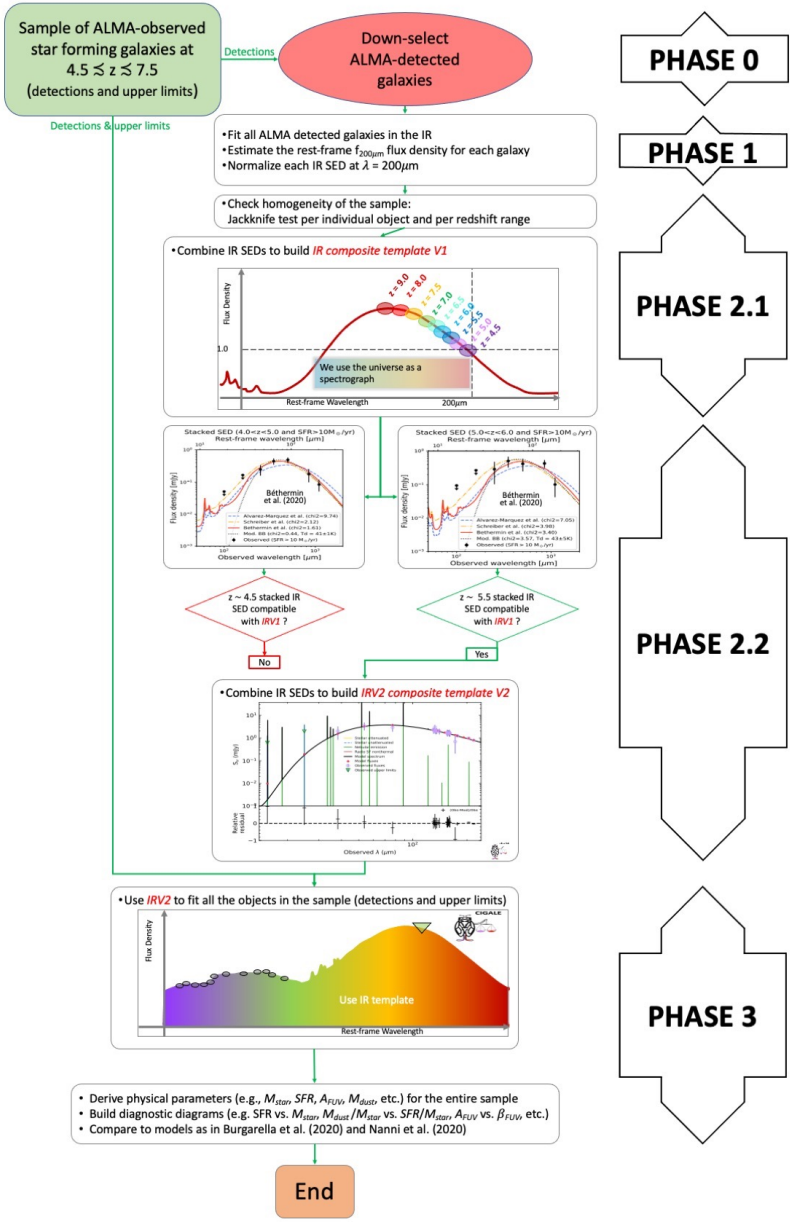

Source	Number of objects	Selection	redshift	Notes
Le Fèvre et al. (2020); Faisst et al. (2020); Bethermin et al. (2020)	118	SFG	z ~ 4.5 z ~ 5.5	* 20 ALMA-7 detections with S/N > 3 * 78 ALMA-7 upper limits * 18 ALMA-7 not selected (not enough data) * $S/N_{UV-optical-NIR} > 2.5$. * SFG with > 5 data points in UV-optical only * [CII]158μm measurements for 64% of the sample
Capak et al. (2015) & Faisst et al. (2017)	4 (HZ4, HZ6, HZ9, HZ10	UV	z ~ 5.6	* [CII]158μm for all Hi-z LBGs * ALMA-7 detections: HZ4, HZ6 (3) HZ9 & HZ10 (5) * ALMA-7 upper limits for the others * HZ5 detected in Chandra and not included in the sample * Additional data from Pavesi et al. (2016)
Scoville et al. (2016)	1 (566428)	UV	z = 5.89	* ALMA-6 detection * [CII]158μm measurement
Willott et al. (2015)	2 (CLM1 & WMH5)	UV	z ~ 6.1	* ALMA-6 detections * [CII]158μm measurement

Table 1: Origins of the data used in this paper. The total sample contains 27 objects with ALMA detections, including 7 LBGs from Burgarella et al. (2020), out of a total sample of 124 objects. The final sample used in this paper contains 105 objects (27 with ALMA detections, 78 with ALMA upper limits and 18 without enough data in the UV-optical-near-IR range to perform a safe SED fitting).

Crucial to control the homogeneity of the sample

Flowchart of the project

- A delayed SFH without burst and tau_main=500 Myrs is noted”tau500”.
- With an additional burst at the end of the SFH, it is noted ”burst”‘.
- A constant SFH without burst and tau_main =20Gyrs is noted "tau20000".
- And when several tau_main could be selected in the SED fitting, it is noted ”multitau” in the legend.

- Top: ΔBIC test that compares the influence of the DL2014 model and the PL+OT_MBB dust emissions in building the IR template.
- Center: ΔBIC test on the SFH assuming the PL+OT_MBB fort he IR template.
- Bottom: ΔBIC test on the SFH assuming the DL2014 model for the IR template.

- The colors band allows to interpret the results of the evidence (ΔBIC) against the model with the higher BIC: red means "faint evidence", orange means "positive evidence" and green mean "strong evidence".
- We do not see any strong evidence that DL2014 or PL+OT_MBB are better to fit the data.
- An SFH that includes a burst is positively ruled out while a delayed SFH with tau_main=500 Myrs is weekly favoured.

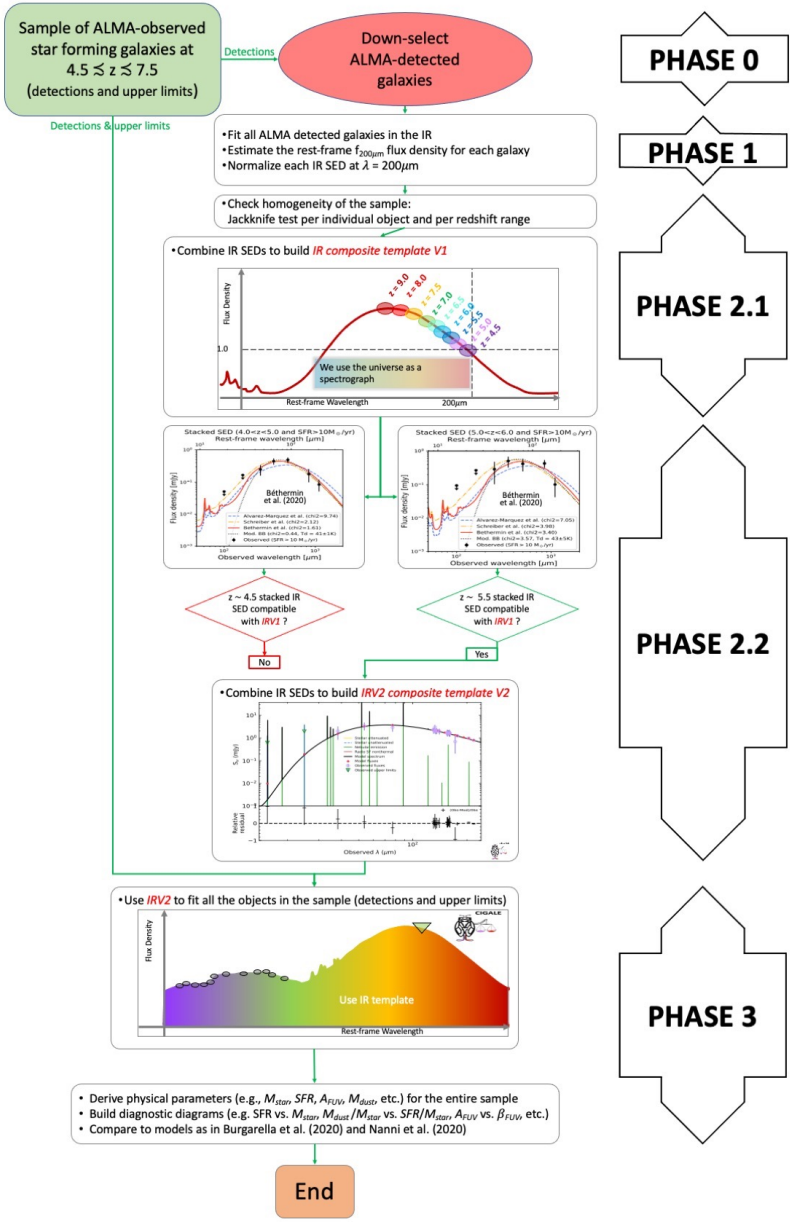

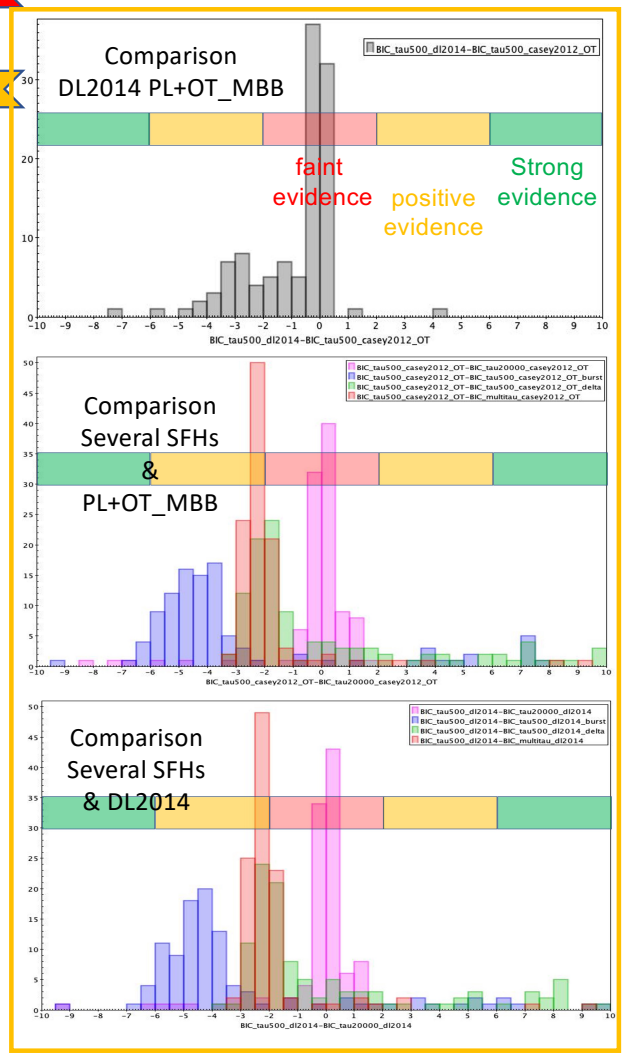

Flowchart of the project

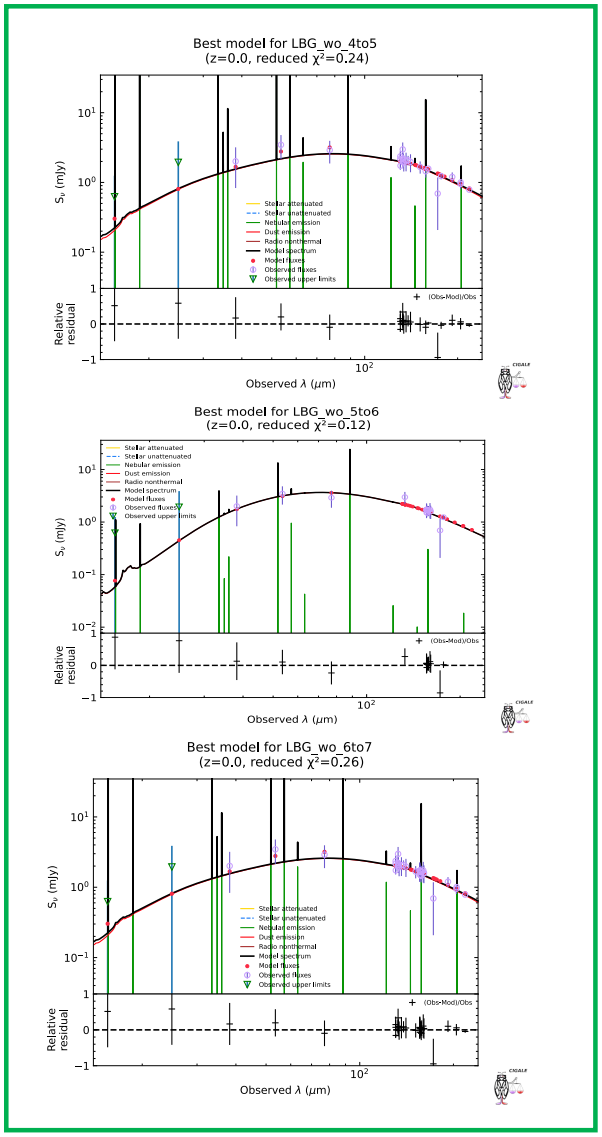

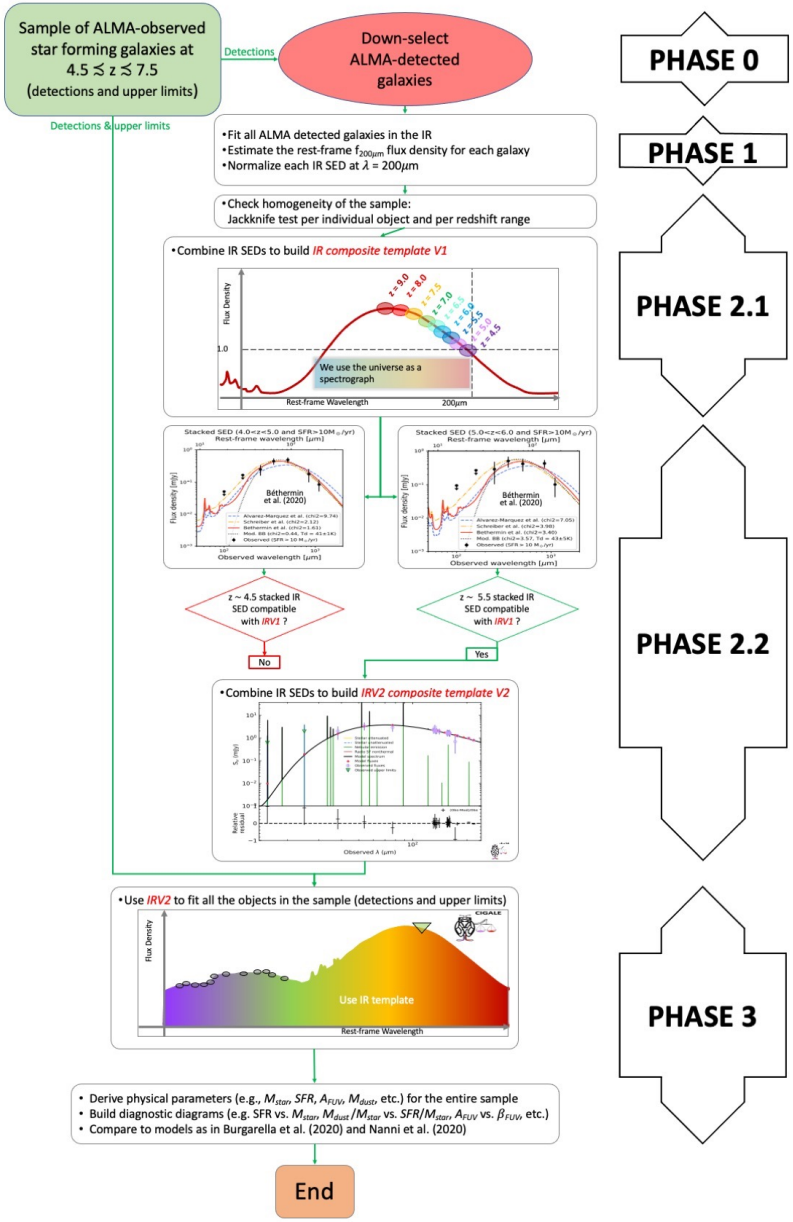

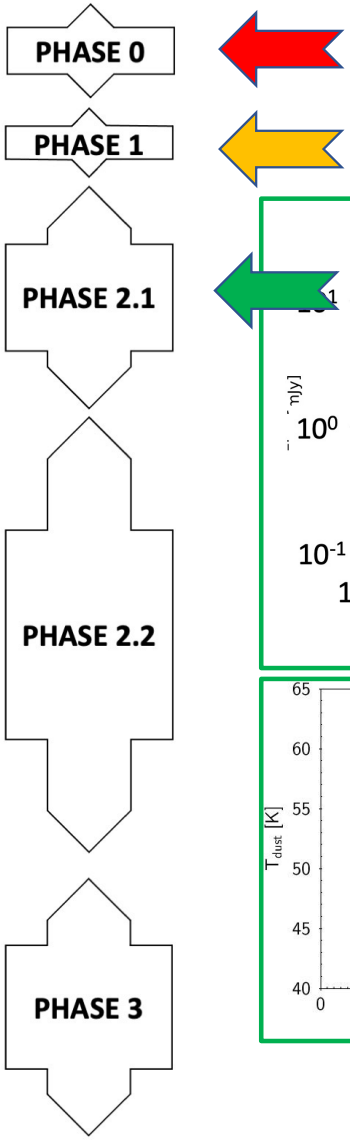

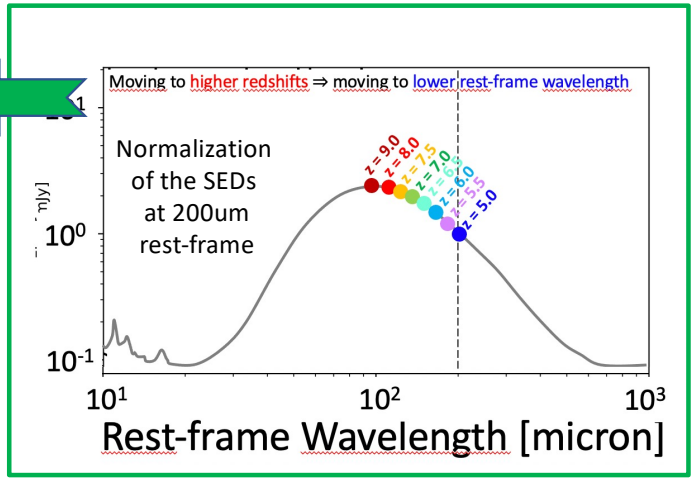

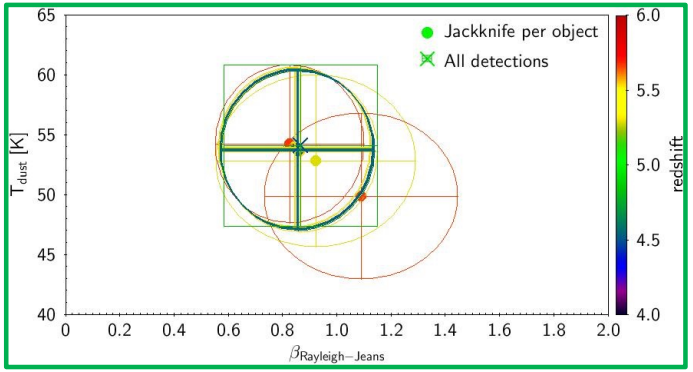

Flowchart of the project

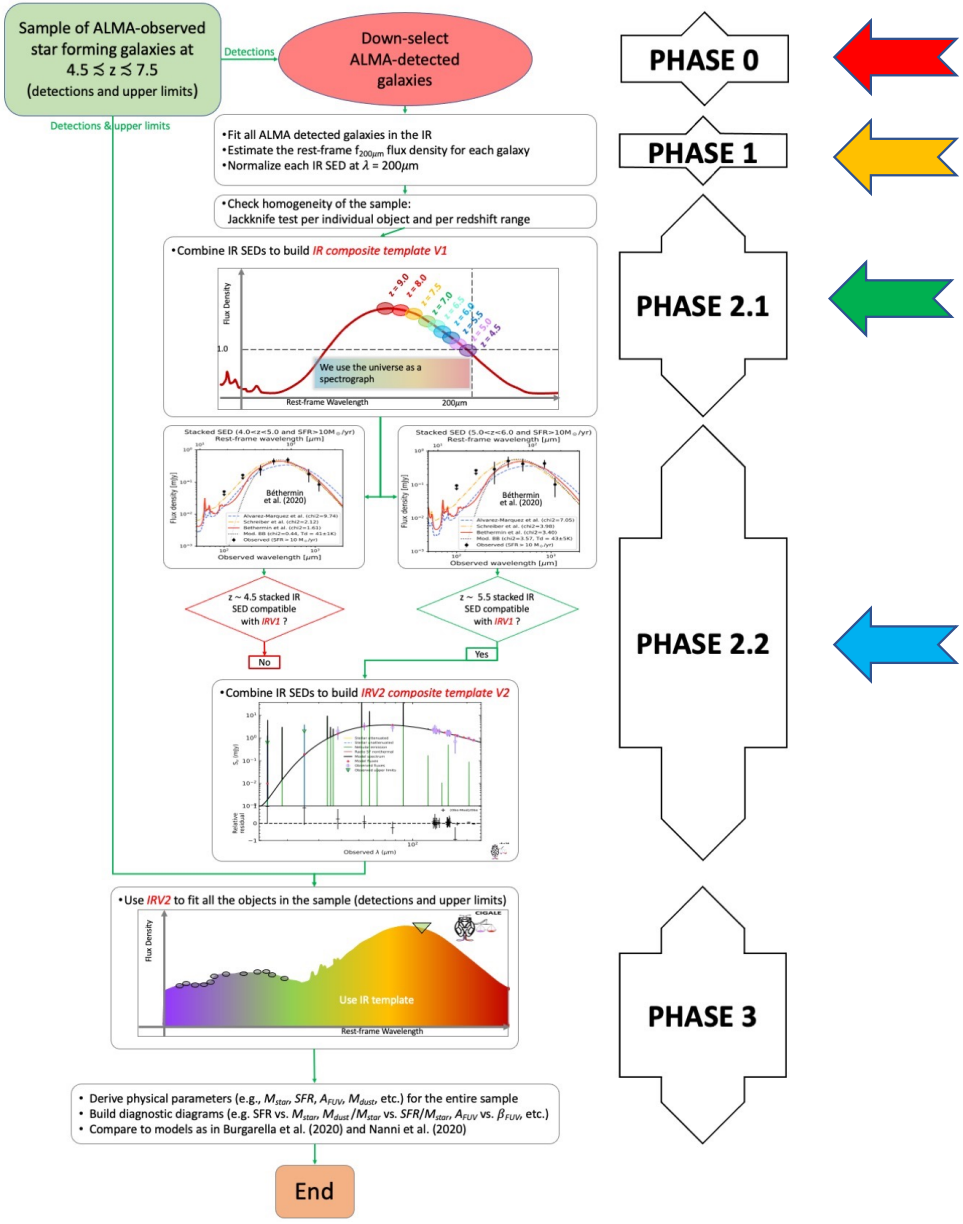

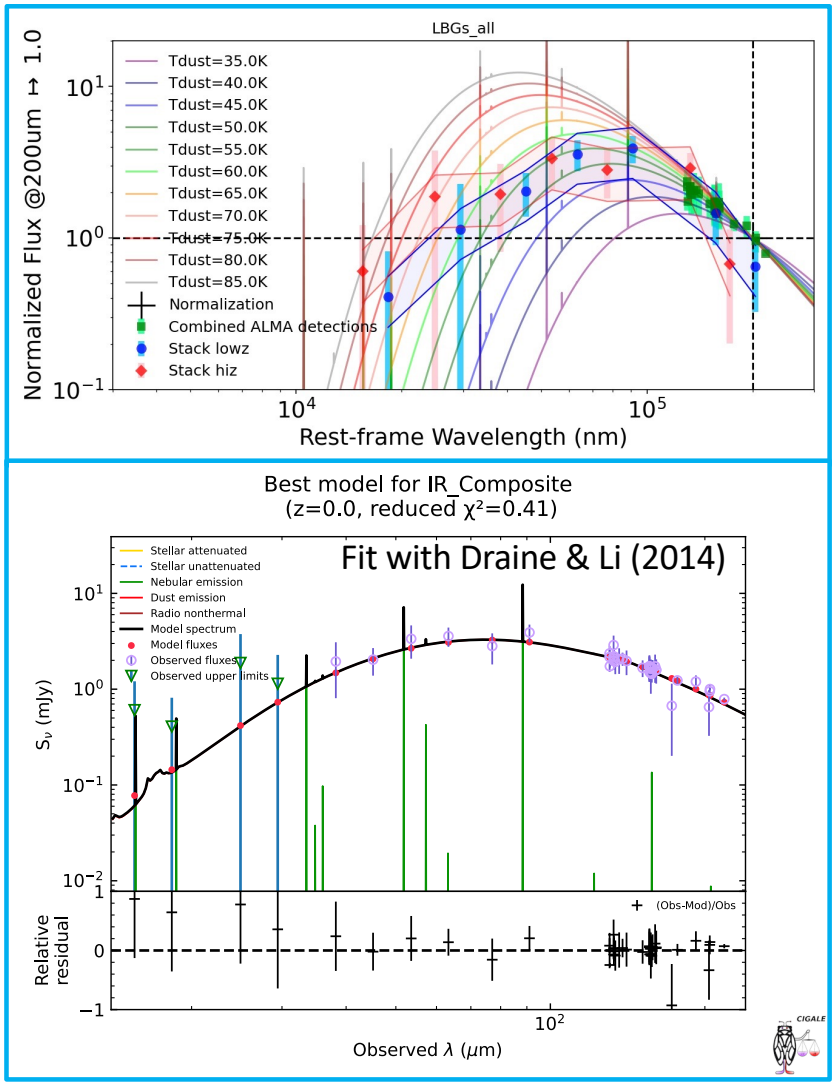

All fits of the IR composite template

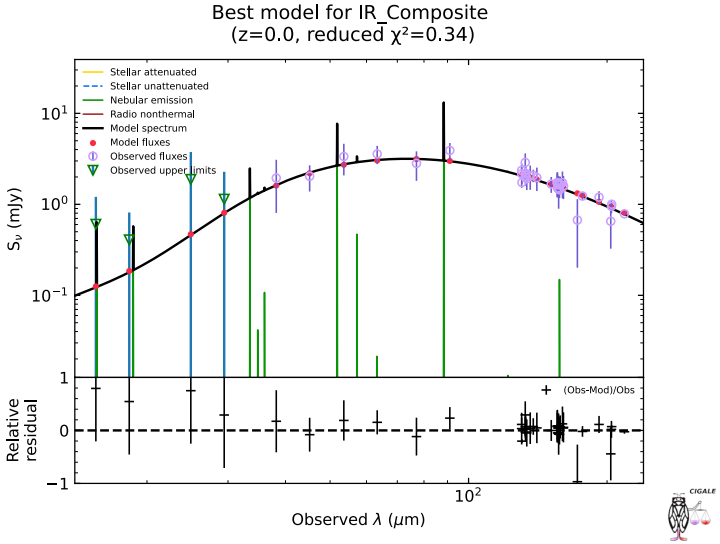

MIR Power Law +
General Modified Blackbody

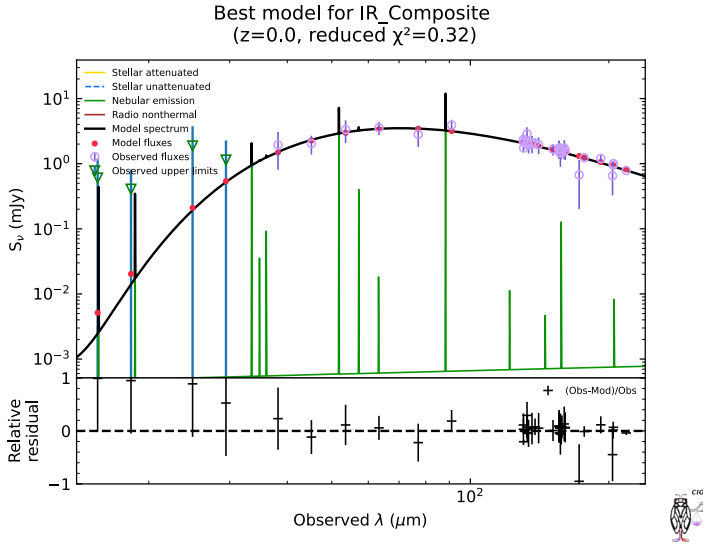

MIR Power Law +
Optically-Thin Modified Blackbody

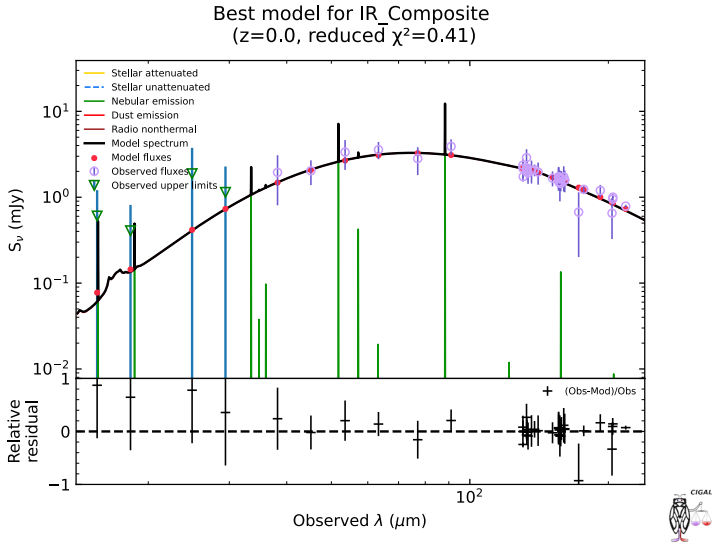

Draine & Li (2014)

Flowchart of the project

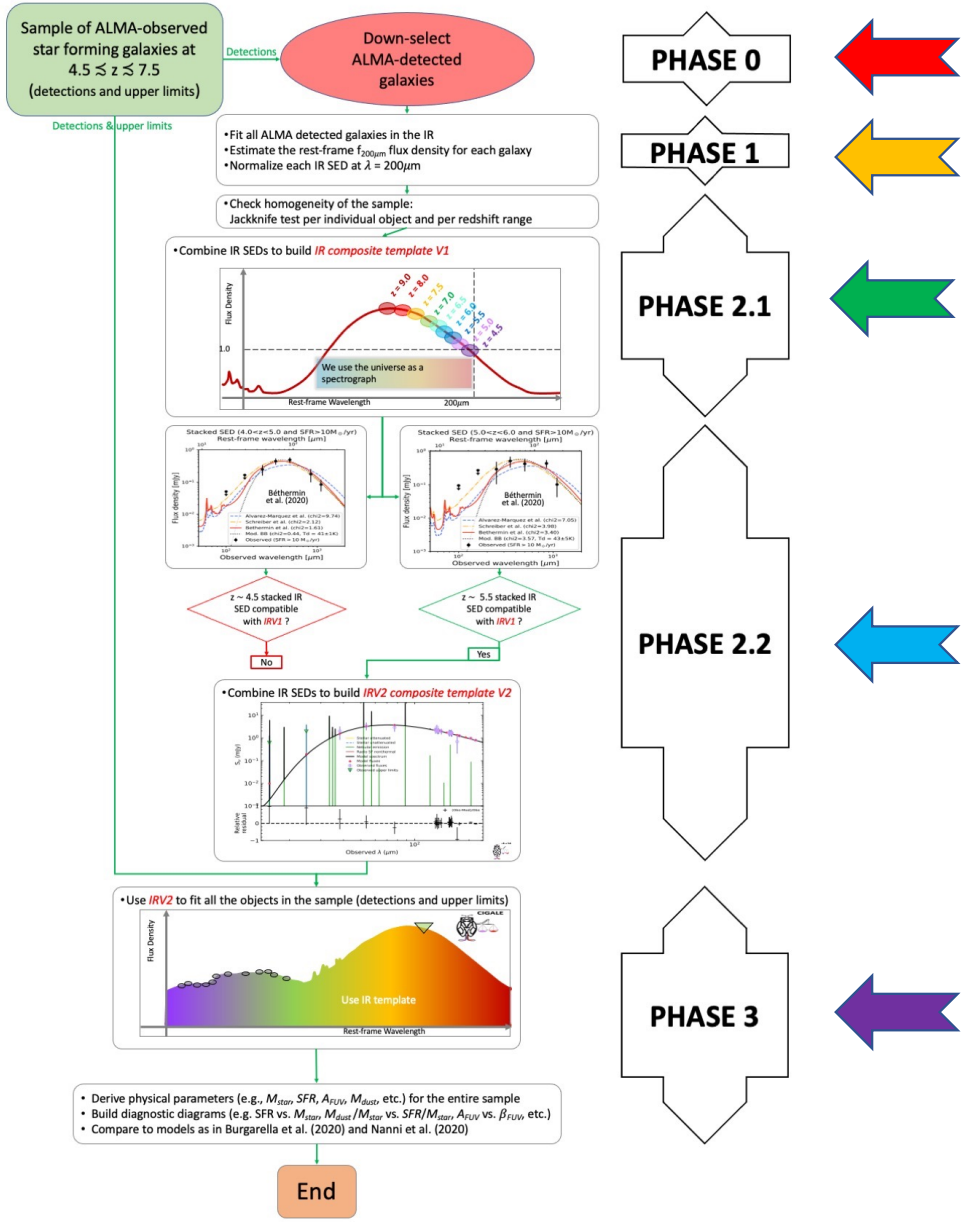

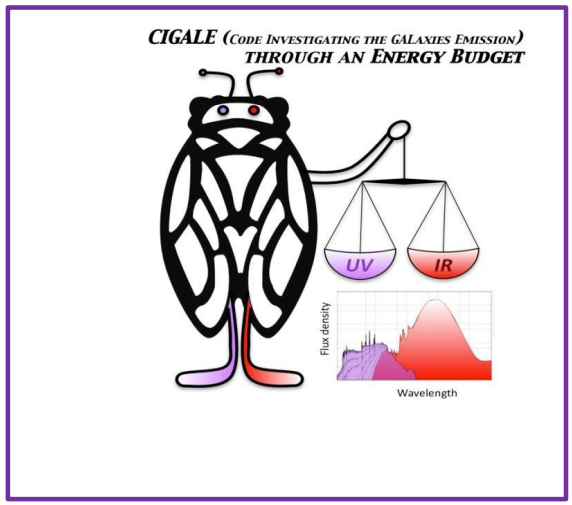

Flowchart of the project

We fit, with CIGALE, all the galaxies in the sample: detections and upper limits

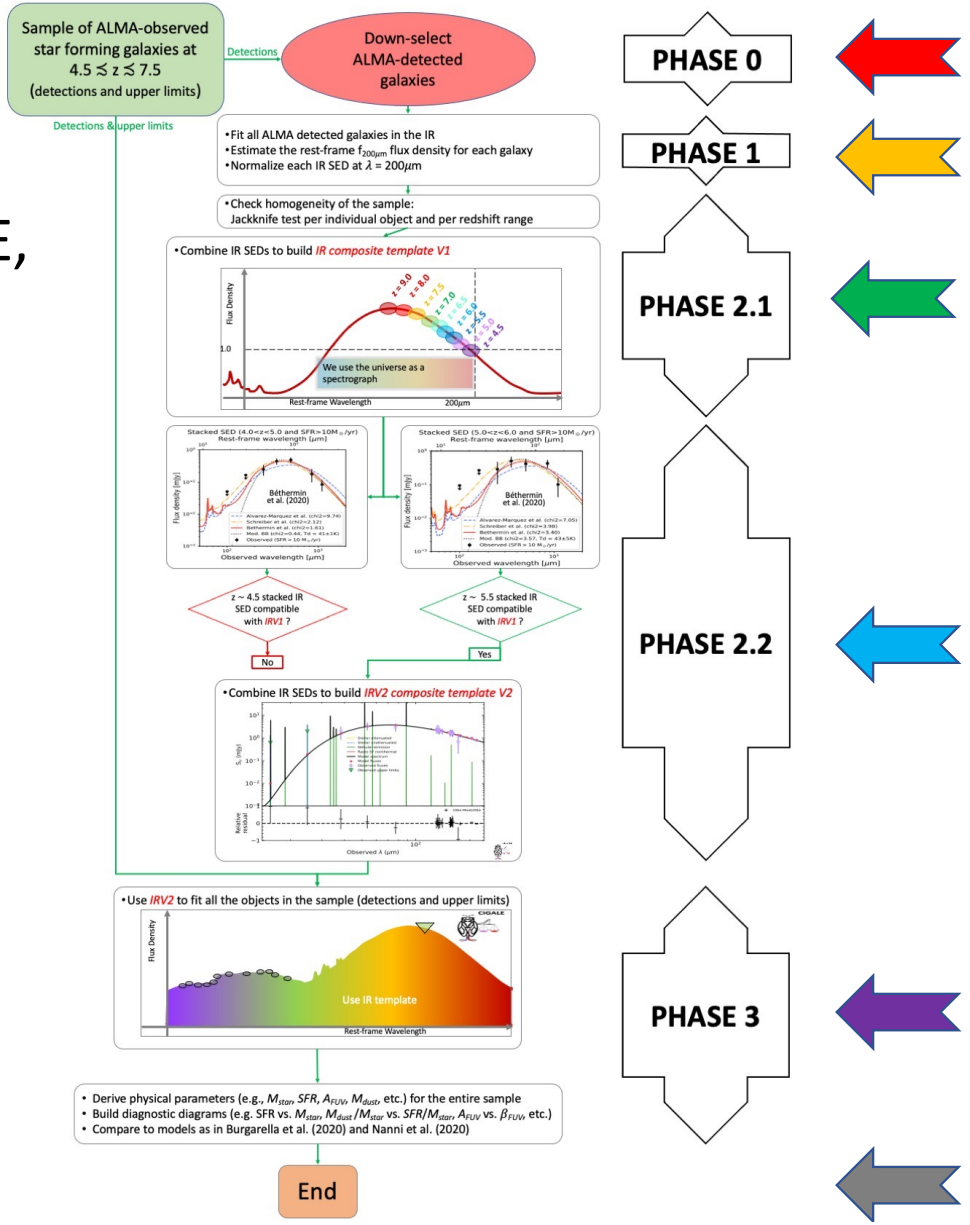

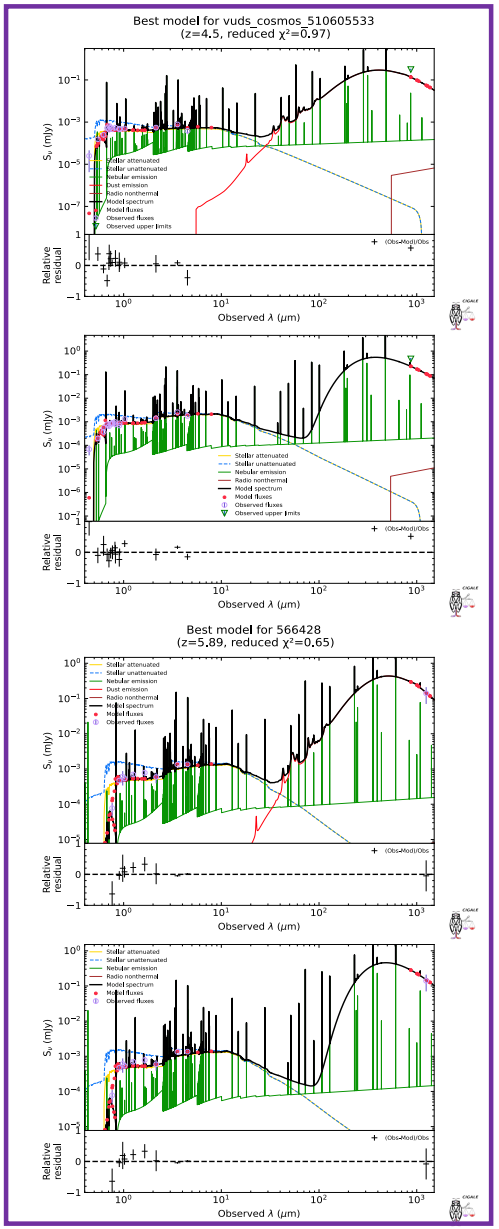

Flowchart of the project

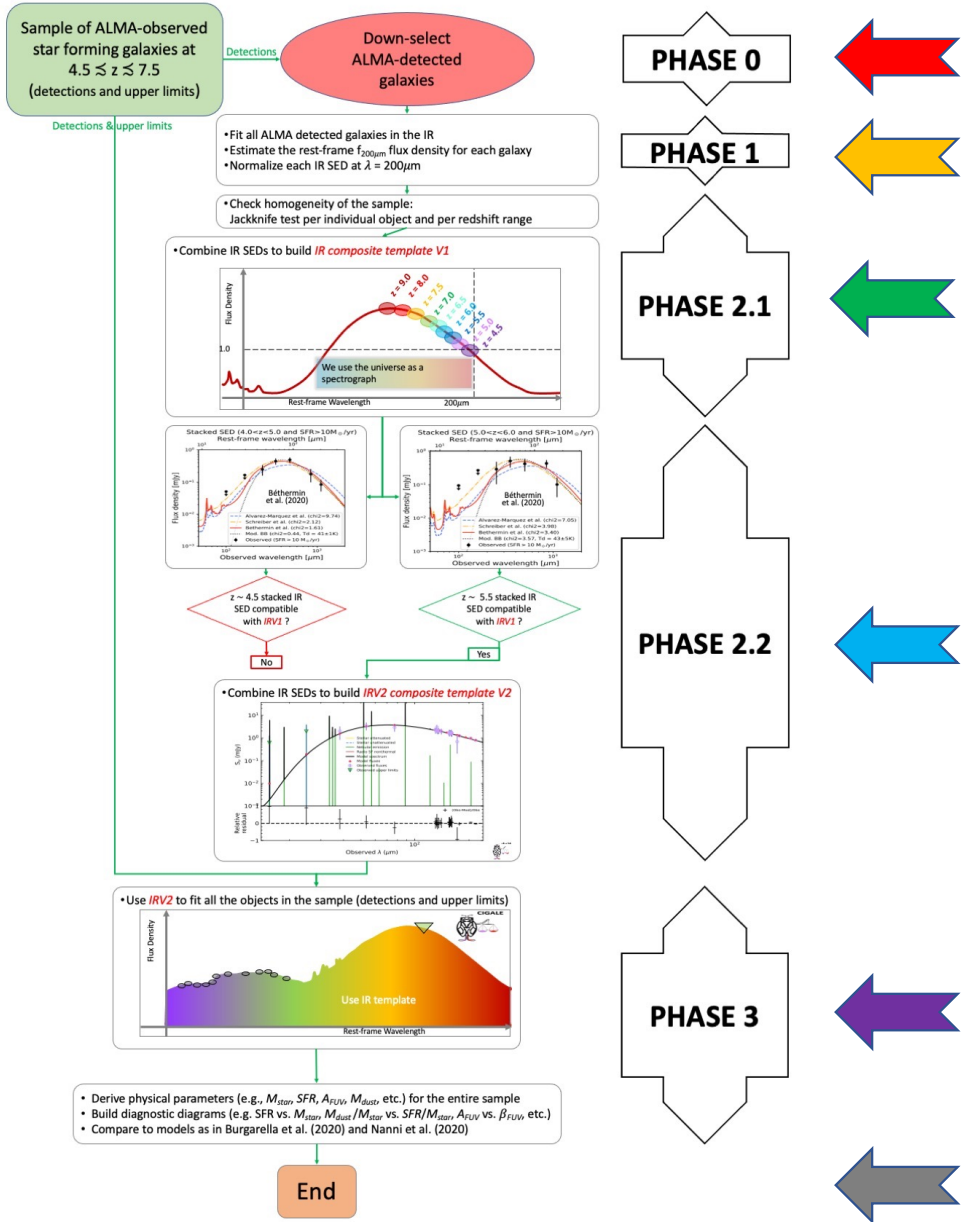

Results

Parameter	*DL2014*	*PL + OT_MBB*
$M_{star}\ [M_\odot]$	$(1.18 \pm 0.19) \times 10^{10}$	$(1.18 \pm 0.18) \times 10^{10}$
$SFR\ [M_\odot\ yr^{-1}]$	47.6 ± 5.1	46.8 ± 5.0
$M_{dust}\ [M_\odot]^*$	$(5.64 \pm 0.69) \times 10^7$	$(2.07 \pm 0.25) \times 10^7$
$L_{dust}\ [L_\odot]$	$(3.38 \pm 0.41) \times 10^{11}$	$(3.32 \pm 0.40) \times 10^{11}$
$L_{FUV}\ [L_\odot]$	$(1.07 \pm 0.06) \times 10^{11}$	$(1.06 \pm 0.06) \times 10^{11}$
$sSFR\ [yr^{-1}]$	$(1.16 \pm 0.34) \times 10^{-8}$	$(1.15 \pm 0.34) \times 10^{-8}$
$sM_{dust}{}^*$	0.010 ± 0.003	0.004 ± 0.001
IRX	0.31 ± 0.14	0.31 ± 0.13
A_{FUV}	1.14 ± 0.15	1.14 ± 0.15
$age_{main}\ [Myr]$	440 ± 98	444 ± 98

Table 6: Mean value and standard deviations of the physical parameters derived from the fit analysis of the individual objects in our sample. The Bayesian outputs are listed here. *The values listed in the table are those computed with $\kappa_0 = 0.637\ m^2 kg^{-1}$ corresponding to Draine et al. (2014). For $\kappa_0 = 0.45\ m^2 kg^{-1}$ [$\kappa_0 = 0.72\ m^2 kg^{-1}$, resp.], that is before [after, resp.] the reverse shock, we have: $M_{dust} = (2.91 \pm 0.35) \times 10^7\ M_\odot$ [$M_{dust} = (1.82 \pm 0.22) \times 10^7\ M_\odot$, resp.] and $sM_{dust} = 0.005 \pm 0.002$ [$sM_{dust} = 0.003 \pm 0.001$, resp.].

- Properties of the IR composite template
- SFR vs. M_{star}
- A_{FUV} vs. M_{star}
- IRX vs. β_{FUV}
- sM_{dust} vs. sSFR (Dust Formation Rate Diagram = DFRD)

- Properties of the IR composite template
- SFR vs. M_{star}
- A_{FUV} vs. M_{star}
- IRX vs. β_{FUV}
- sM_{dust} vs. sSFR (DFRD)

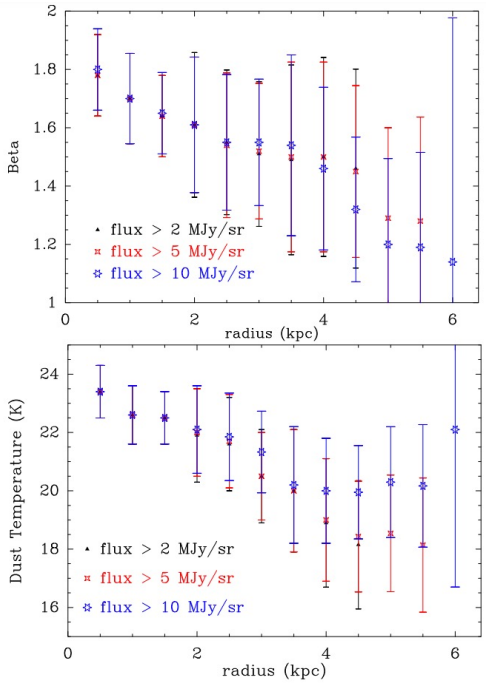

Fig. 3. Radial variation of the 'best-β' calculated by minimizing the reduced χ^2 for each of the annuli in the single modified black body (MBB) fitting approach (*top*). The different symbols show a coherent decrease in β with radius and represent values obtained for different flux cutoffs as indicated. (*Bottom*): dust temperature calculated for each flux cutoff at each radius. The error bars show the 1 sigma dispersion.

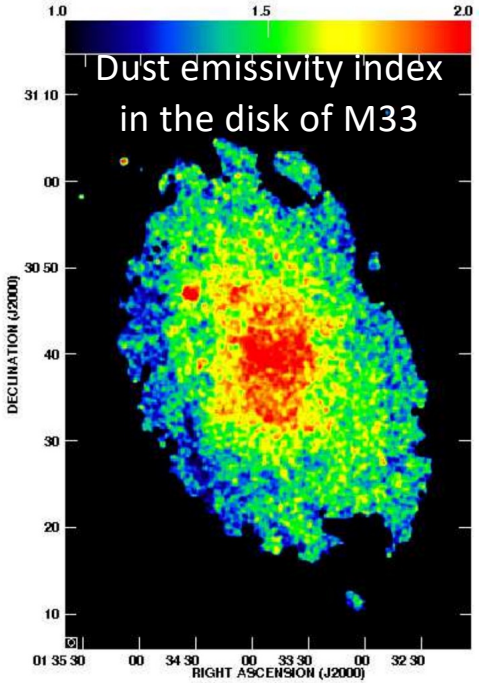

Tabatabaei (2014A&A...561A..95T):
The mean value of the dust emissivity index over the disk is β = 1.5 ± 0.2.

	PL+G_MBB	PL+OT_MBB	DL2014
α_{MIR}	2.23±0.63	2.00±0.82	N/A
β_{RJ}	1.43±0.47	0.87±0.28	N/A
T_{dust}[K]	65.5±5.1	54.1±6.7	N/A
q_{PAH}	N/A	N/A	0.47
α	N/A	N/A	2.39±0.44
u_{min}	N/A	N/A	18.1±12.7
γ	N/A	N/A	0.54±0.35
$L_{dust}/10^{20}$ [W]	2.84±0.14	2.43±0.12	2.57±0.13

Table 3: Main relevant physical parameters derived by fitting the IR template with the various assumptions of the dust emission: PL+G_MBB is based on a power law in the mid IR plus the general blackbody formula as in Casey et al. (2012), PL+OT_MBB is a power-law in the mid IR (α_{MIR}) plus an optically thin blackbody, again similar to Casey et al. (2012) and DL2014 stands for Draine & Li (2014) models (the parameters for DL2014 are described in Appendix A). Because the SEDs are normalized to 1.0 at $\lambda = 200\mu m$, the values of L_{dust} can be directly compared.

- Properties of the IR composite template
- SFR vs. M_{star}
- A_{FUV} vs. M_{star}
- IRX vs. β_{FUV}
- sM_{dust} vs. sSFR (DFRD)

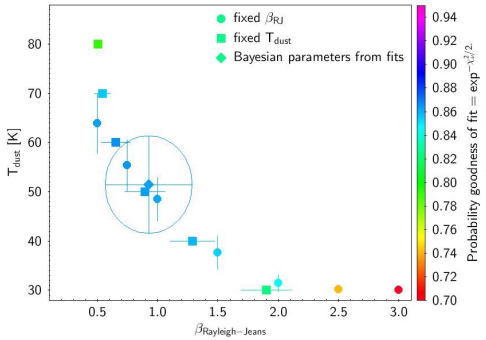

Bakx et al. (2021MNRAS.508L..58B)

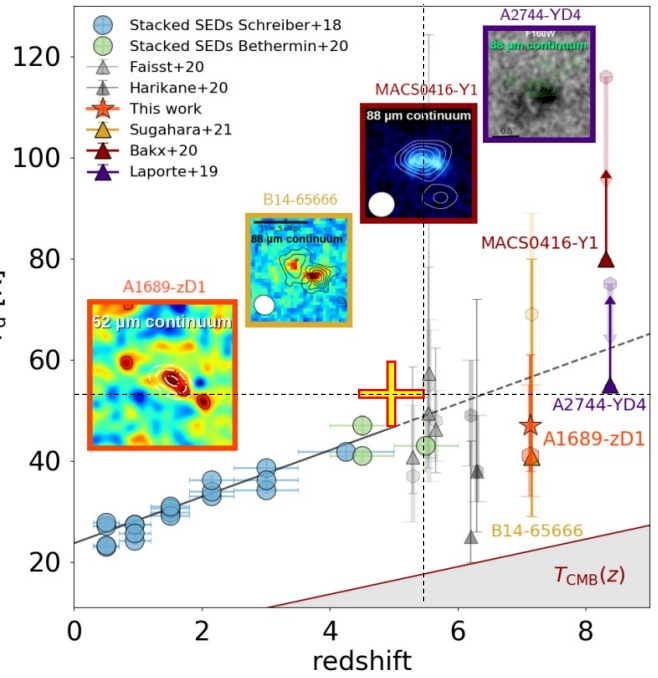

Figure 4. Dust temperature T_d in "normal" (main-sequence) galaxies as a function of redshift. The newest T_d estimates for A1689-zD1 are shown in *red* (*star* for SED-fit and *hexagon* for the [C II]-based result). Dust temperatures obtained from stacked SEDs (*blue and green circles*) increase linearly with redshift up to $z = 6$. We highlight all the continuum detected sources at $z > 7$ with small post-stamps, and include their estimated T_d based on both SED fits (*triangles*) and the [C II]-based method (*hexagons*; Faisst et al. 2020; Harikane et al. 2020; Sugahara et al. 2021; Bakx et al. 2020; Laporte et al. 2019). The addition of band 9 data significantly reduces the uncertainty on the dust temperature of this source with respect to the other high-z sources, which are not observed in that band.

	PL+G_MBB	PL+OT_MBB	DL2014
α_{MIR}	2.23±0.63	2.00±0.82	N/A
β_{RJ}	1.43±0.47	0.87±0.28	N/A
T_{dust}[K]	65.5±5.1	54.1±6.7	N/A
q_{PAH}	N/A	N/A	0.47
α	N/A	N/A	2.39±0.44
u_{min}	N/A	N/A	18.1±12.7
γ	N/A	N/A	0.54±0.35
$L_{dust}/10^{20}$ [W]	2.84±0.14	2.43±0.12	2.57±0.13

Table 3: Main relevant physical parameters derived by fitting the IR template with the various assumptions of the dust emission: PL+G_MBB is based on a power law in the mid IR plus the general blackbody formula as in Casey et al. (2012), PL+OT_MBB is a power-law in the mid IR (α_{MIR}) plus an optically thin blackbody, again similar to Casey et al. (2012) and DL2014 stands for Draine & Li (2014) models (the parameters for DL2014 are described in Appendix A). Because the SEDs are normalized to 1.0 at $\lambda = 200\mu m$, the values of L_{dust} can be directly compared.

- Properties of the IR composite template
- SFR vs. M_{star}
- A_{FUV} vs. M_{star}
- IRX vs. β_{FUV}
- sM_{dust} vs. sSFR (DFRD)

- Schulz et al. (2020) suggests an evolution of the intrisic UV slope with redshift in range 0 < z < 4
- Extrapolated to higher redshifts does not seem to work
- We need to calibrate the evolution with redshift, or more physically with mass-weighted age of the stellar populations.

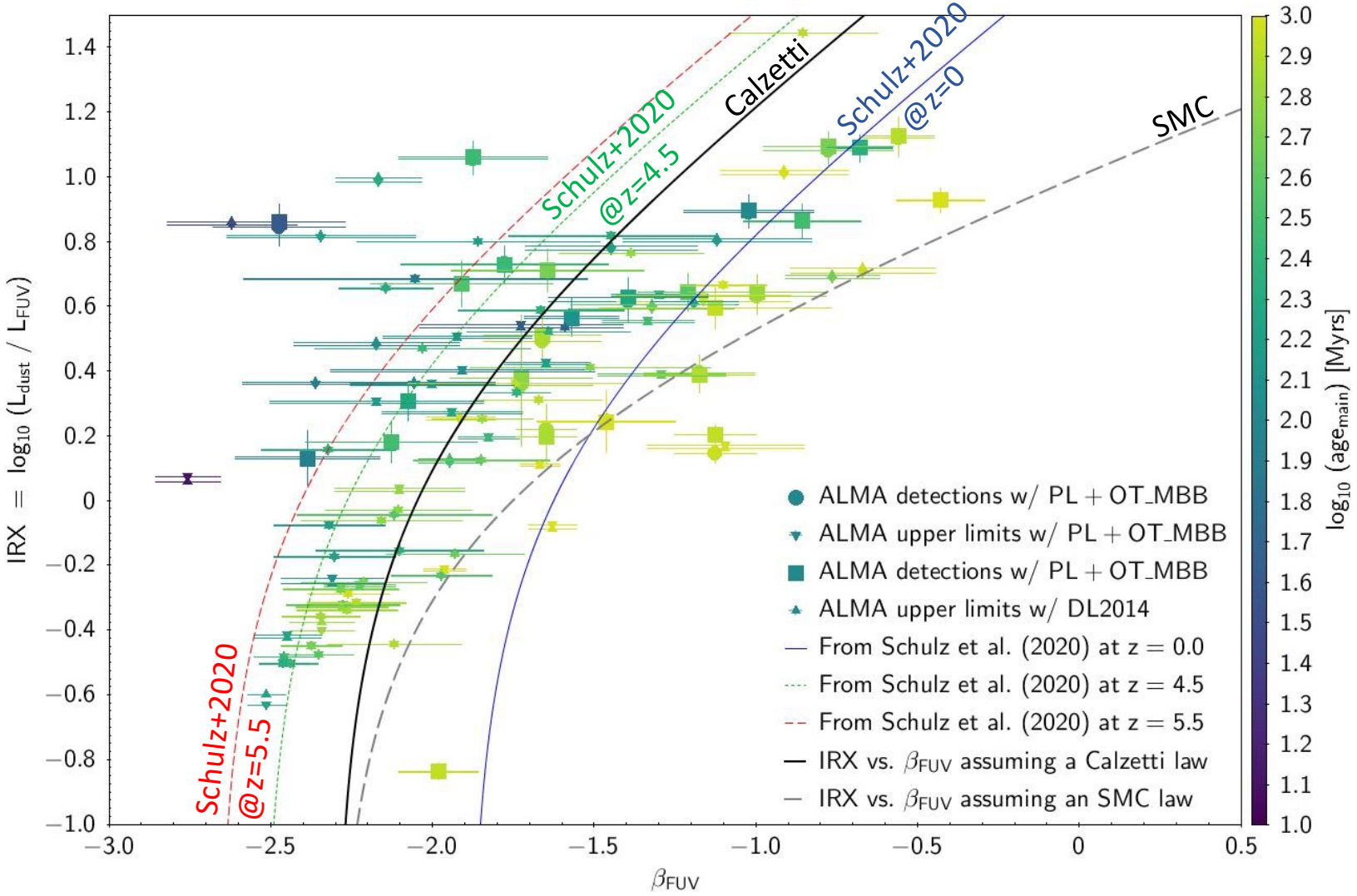

- Properties of the IR composite template
- SFR vs. M_{star}
- A_{FUV} vs. M_{star}
- IRX vs. β_{FUV}
- sM_{dust} vs. sSFR (DFRD)

- Schulz et al. (2020) suggests an evolution of the intrisic UV slope with redshift in range $0 < z < 4$
- Extrapolated to higher redshifts does not seem to work
- We need to calibrate the evolution with redshift, or more physically with mass-weighted age of the stellar populations.

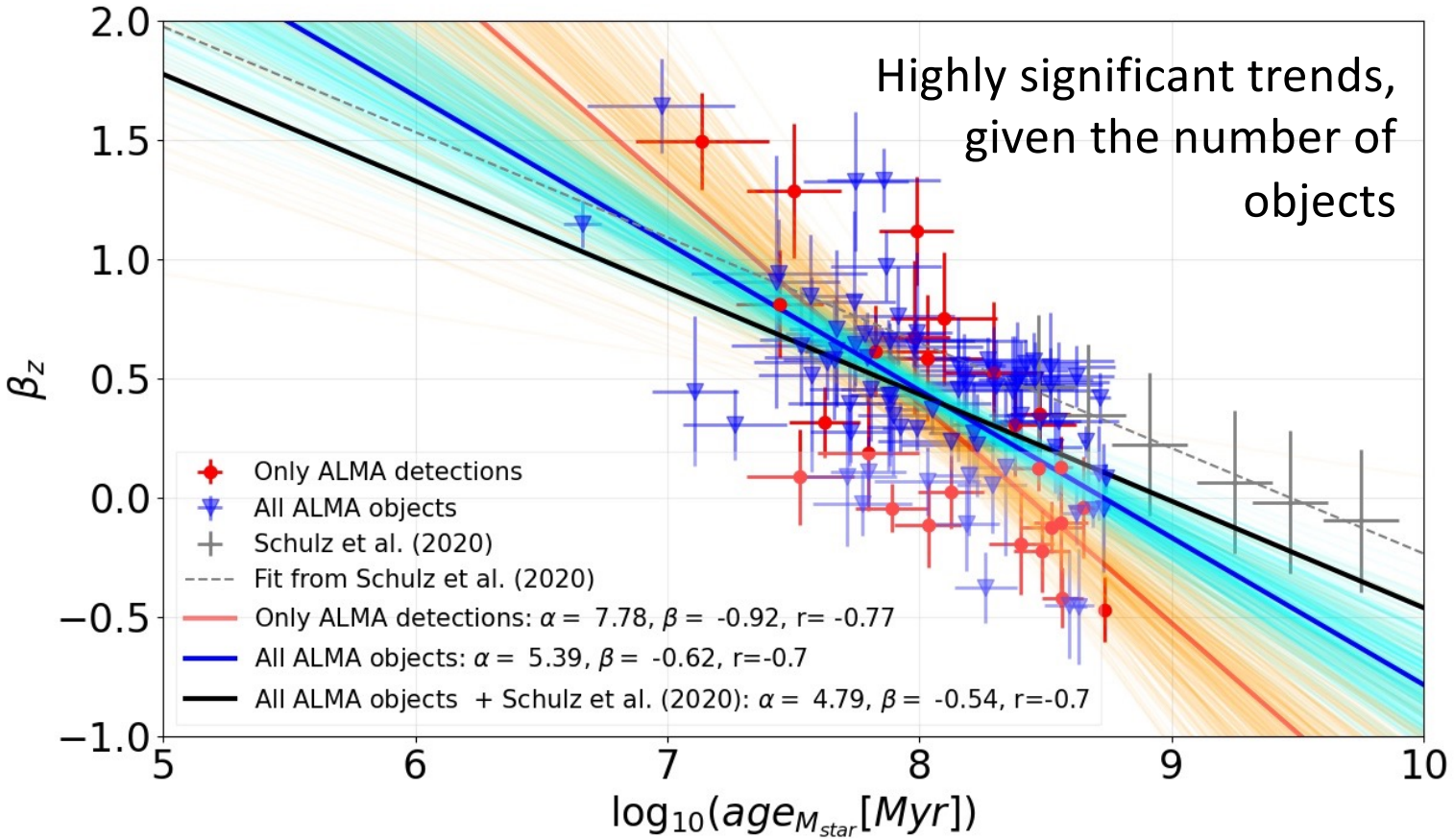

- Properties of the IR composite template
- SFR vs. M_{star}
- A_{FUV} vs. M_{star}
- IRX vs. β_{FUV}
- sM_{dust} vs. sSFR (DFRD)

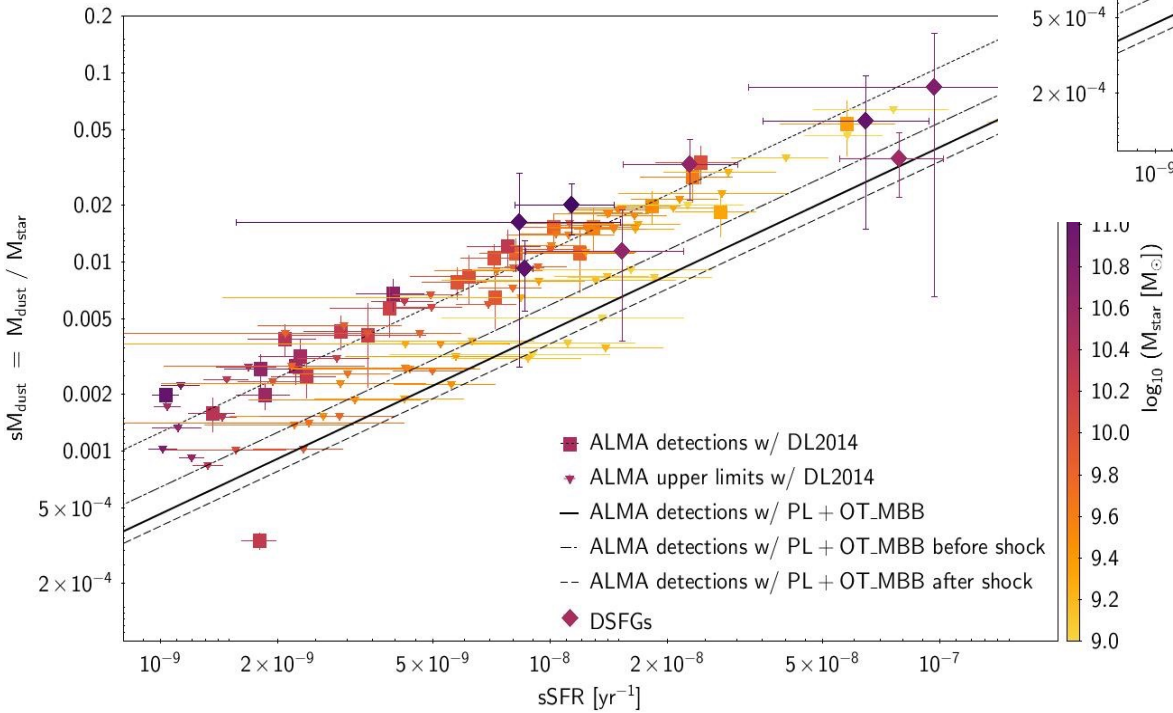

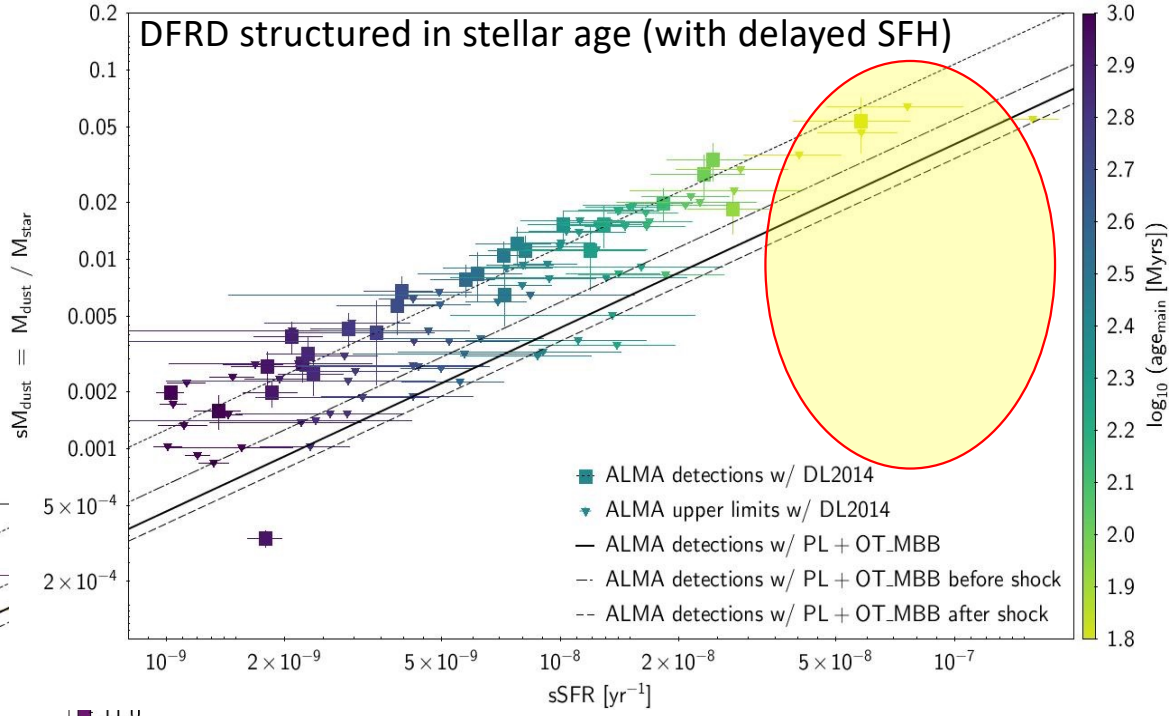

- Distant dusty star forming galaxies seem to follow the same trend than low-M_{star} + low-A_{FUV} galaxies in the DFRD.
- However the stellar masses of these objects significantly differ from the low-M_{star} + low-A_{FUV} sample.
- High sSFR region reach very high sM_{dust}.
- Low density of objects => fast dust formation and evolution.

- Properties of the IR composite template
- SFR vs. M_{star}
- A_{FUV} vs. M_{star}
- IRX vs. β_{FUV}
- sM_{dust} vs. sSFR (DFRD)

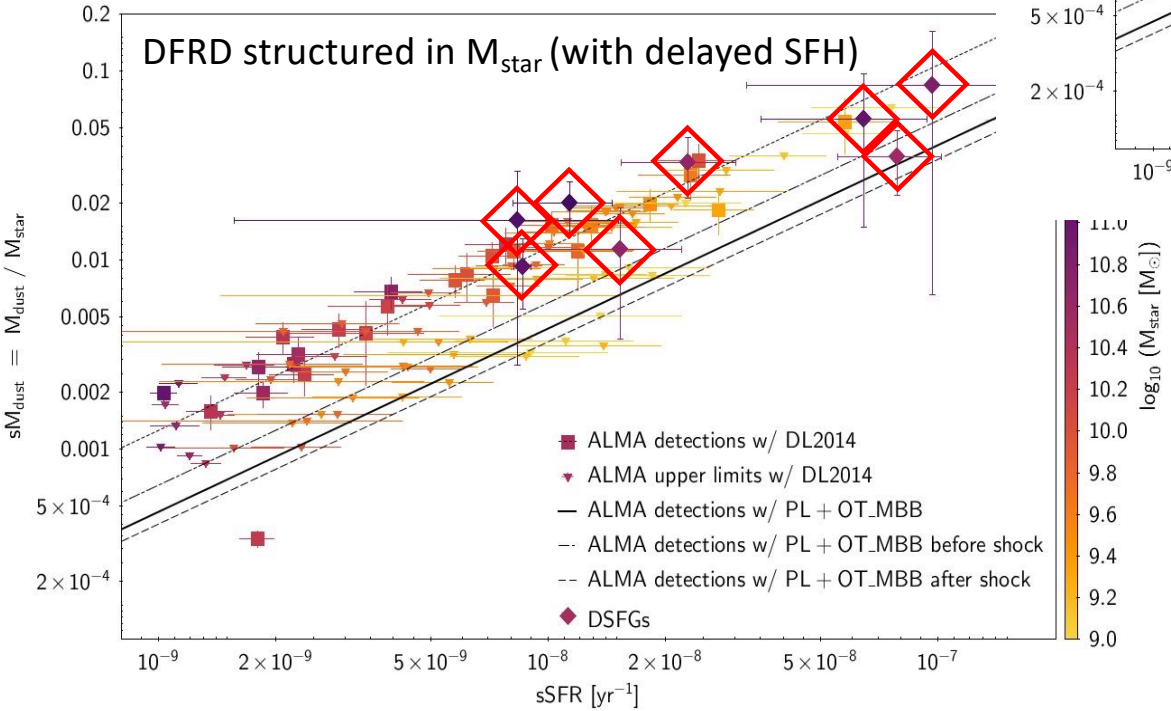

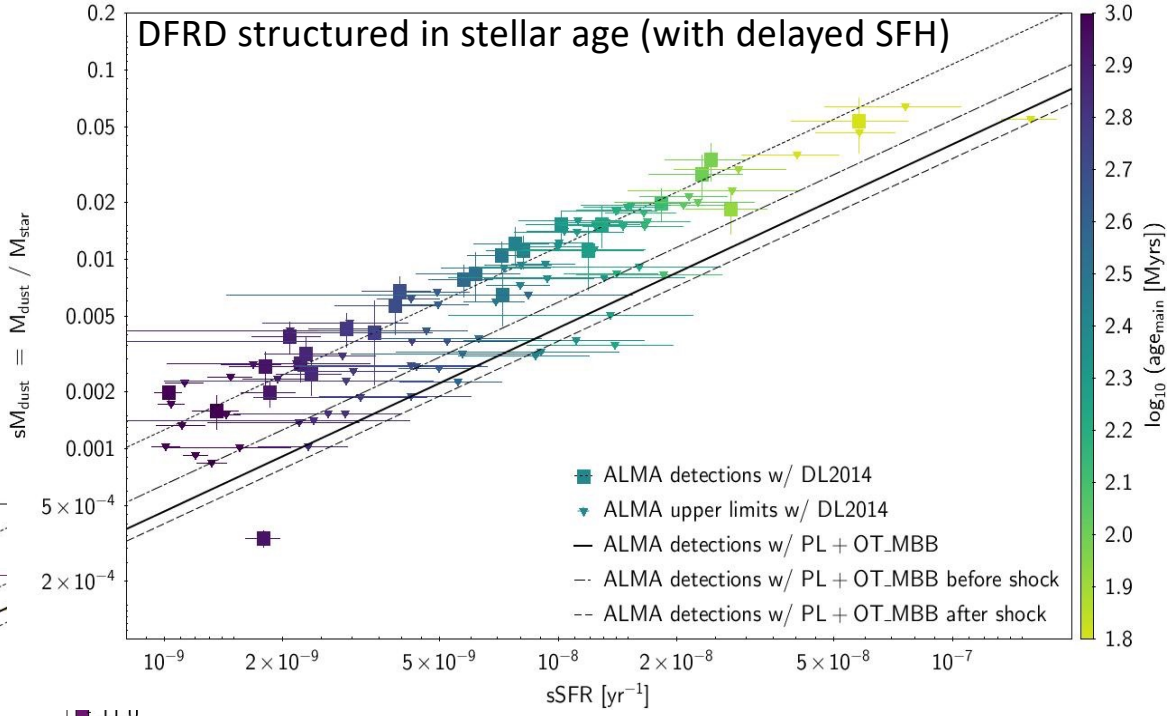

- Distant dusty star forming galaxies seem to follow the same trend than low-M_{star} + low-A_{FUV} galaxies in the DFRD.
- However the stellar masses of these objects significantly differ from the low-M_{star} + low-A_{FUV} sample.
- High sSFR region reach very high sM_{dust}.
- Low density of objects => fast dust formation and evolution.

- Properties of the IR composite template
- SFR vs. M_{star}
- A_{FUV} vs. M_{star}
- IRX vs. β_{FUV}
- sM_{dust} vs. sSFR (DFRD)

- Models hardly explain the high sSFR + high sM_{dust} objects
- How sure are M_{dust}?

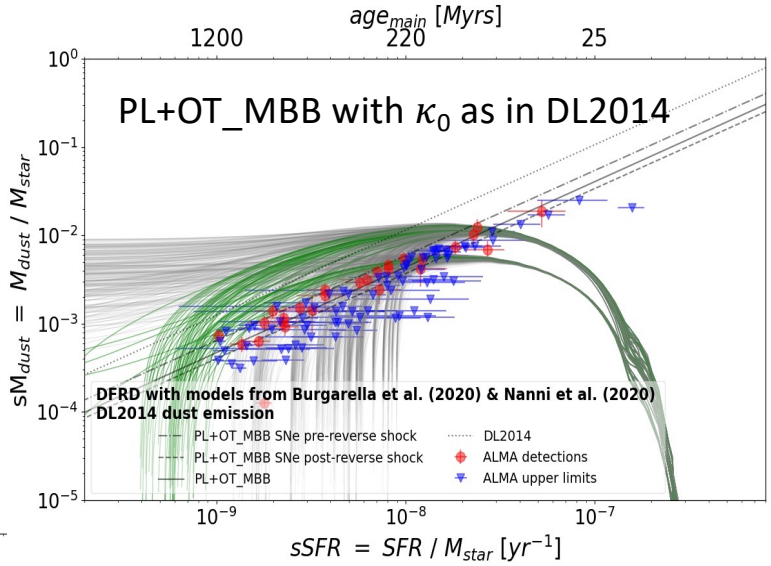

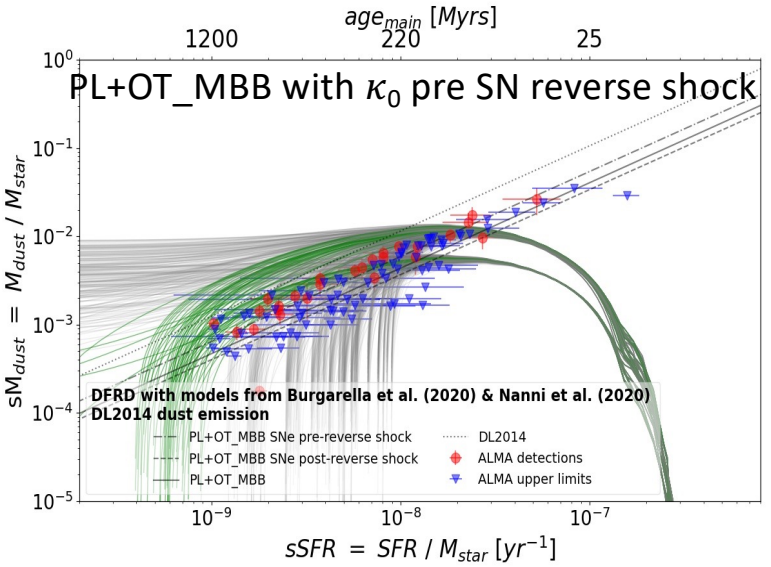

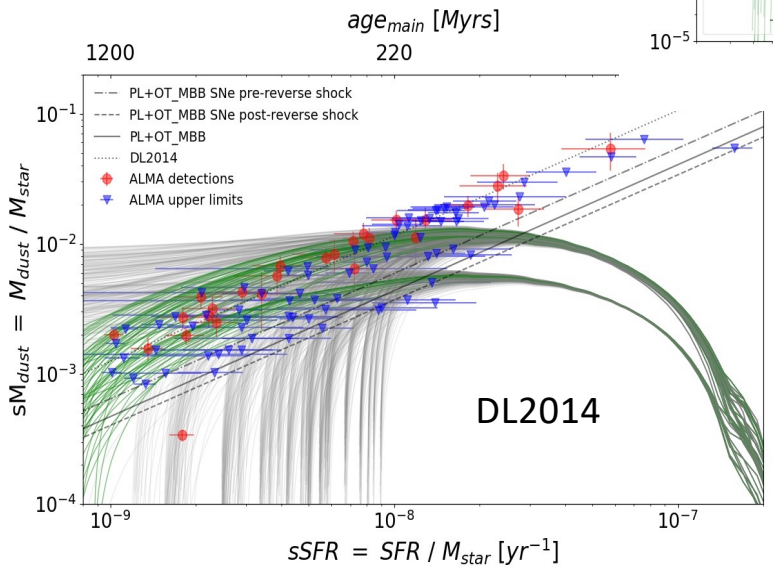

- How sure are M_{dust}?
- $M_{dust} \propto S_\nu / [\ \kappa_\nu B_\nu(T)\ ]$
- An important parameter is
  $\kappa_\lambda = \kappa_0 (\lambda_0/\lambda)^\beta$
- κ_0 = 0.637 m^2/kg for DL2014
- κ_0 = 0.45 m^2/kg for pre-SN reverse shock
- κ_0 = 0.72 m^2/ kg for post-SN reverse shock

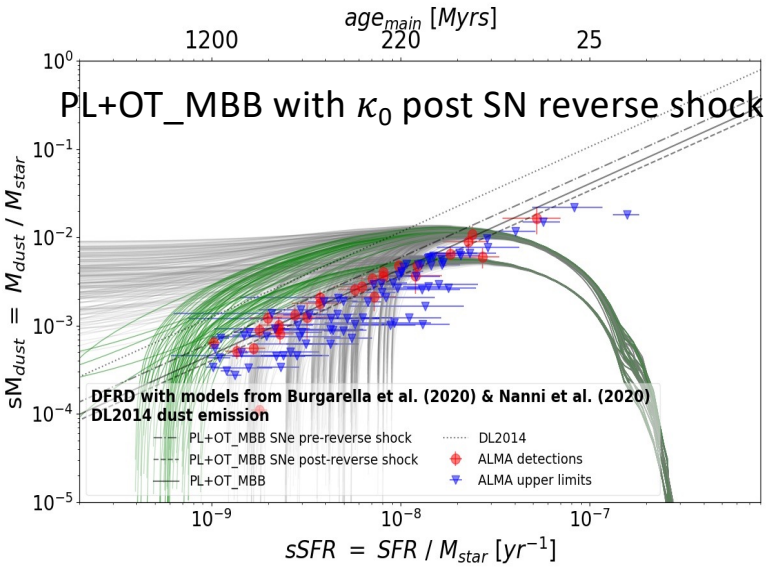

Conclusion(s) et perspective(s)

- We built an IR composite template that should be valid for high redshift star forming galaxies (z > 4.5).
- SFR vs. M_{star} of the sample in agreement with previous works
- A_{FUV} vs. M_{star}: we confirm the evolution in redshift of the relation with apparent $A_{FUV} > 0$ at $\log(M_{star}) < 9.0$
- IRX vs. β_{FUV}: we find an evolution of the intrinsic UV slope β_0 with the age of stellar populations (and redshift).
- sM_{dust} vs. sSFR (DFRD): Estimating M_{dust} is a big issue. We need to populate the high sSFR part of the diagram to constrain the fast formation of dust grains in the early universe.

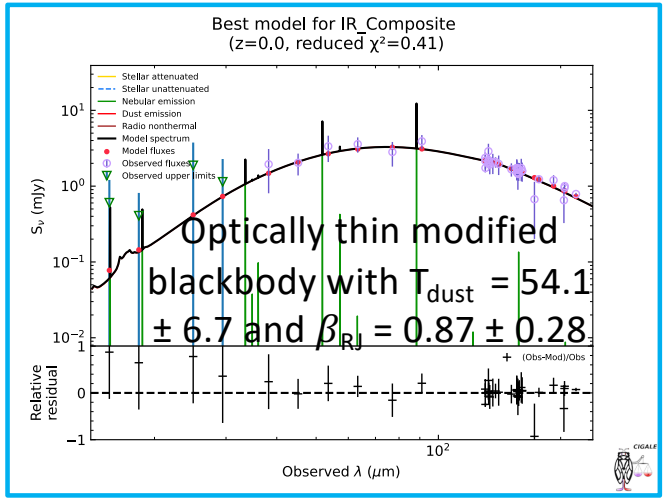

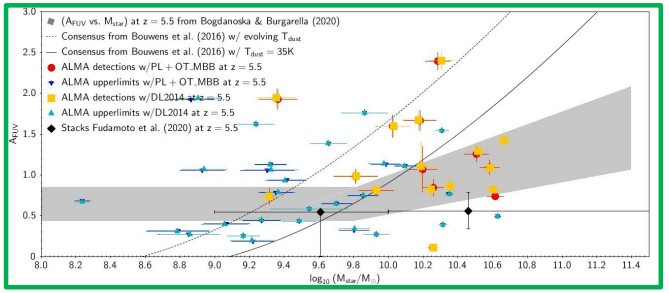

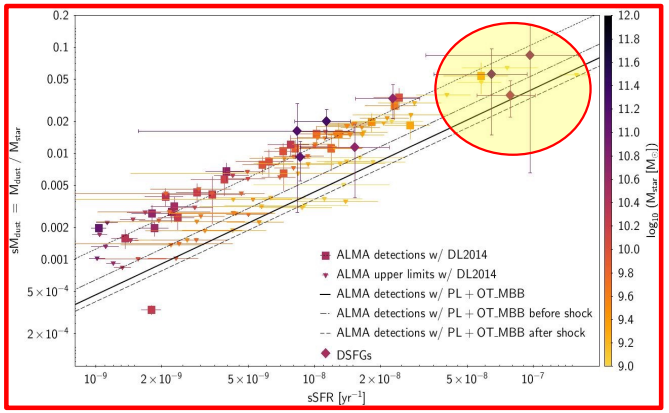

Fin

- Merci

IR fine-structure lines in the South Pole Telescope sample at $2 < z < 7$

- **Context:** we would be very interested to get FIR spectroscopy of about 100 dusty galaxies at high redshift... But we can't...
- **Science objectives:** measure the physical conditions in the ISM at high redshift.
- **Problem:** SED fitting of FIR fluxes hardly can provide estimates of the FIR emission lines.
- I will present a **possible solution** to meet the above science objective.